ELSEVIER

Journal of Fluids and Structures 25 (2009) 229–244

JOURNAL OF FLUIDS AND STRUCTURES

www.elsevier.com/locate/jfs

A numerical investigation of the near-wake structure in the variable frequency forced oscillation of a circular cylinder

S. Atluri[1], V.K. Rao[2], C. Dalton*

Department of Mechanical Engineering, University of Houston, Houston, Texas 77204-4006, USA

Received 29 March 2007; accepted 4 June 2008
Available online 15 October 2008

Abstract

The near-wake structure of a uniform flow past a circular cylinder undergoing a constant-amplitude transverse forced oscillation is studied numerically using a 2-D large eddy simulation (LES) calculation with a Reynolds number range from 500 to 8000. Two effects are considered: First, a comparison is made between the wake structures of periodic and nonperiodic forced oscillations of the cylinder. This was done to emphasize the importance of wake-structure differences of a periodic forced oscillation and a self-excited oscillation of a circular cylinder with the latter being characterized as a nonperiodic forced oscillation. The nonperiodic constant-amplitude forced oscillations were obtained by modulating the frequency of the periodically oscillating cylinder. The differences in the vortex-shedding behavior were made evident by analyzing the vorticity field in the entire wake domain. Second, the effect of changes in the moderate values of the Reynolds number for constant and variable frequency oscillation was investigated. Significant effects on the vortex-shedding patterns in the near wake were observed for both aspects of this study.

Keywords: Computational Fluid Dynamics; Vortex-induced vibration; Forced oscillations; Wake mode response; Variable frequency; Variable Reynolds number; Large eddy simulation

1. Introduction

1.1. Forced oscillation of a circular cylinder

Any motion of a cylinder in a steady approach flow clearly affects the flow field in the wake of the cylinder. The cylinder motion can be in-line with the approach flow direction, transverse to the approach flow direction, or in some combination of the two. The motion of the cylinder can occur from either a forced or free oscillation. The latter type of oscillation is commonly referred to as vortex-induced vibration (VIV). Early studies of VIV were oriented toward studying the effects of the controlled motion of the cylinder on its wake pattern. Several early experiments were conducted on this controlled motion by forcibly oscillating the cylinder at constant amplitude and constant frequency in

*Corresponding author.
E-mail address: dalton@uh.edu (C. Dalton).
[1]Now with Technip, Houston, TX, USA.
[2]Now with Granheme, KBR, Houston, TX, USA.

0889-9746/$ - see front matter © 2009 Elsevier Ltd. All rights reserved.
doi:10.1016/j.jfluidstructs.2008.06.012

the transverse direction. The force on the cylinder due to the fluid flow can be determined by subtracting the inertia force of the cylinder from the force required to oscillate the cylinder.

Bishop and Hassan (1964) investigated experimentally the forces exerted on a cylinder in a forced oscillation over a wide range of frequencies and oscillation amplitudes. Their experiments showed that there was an increase in the magnitude of mean drag and lift amplitude when the excitation frequency approaches the natural shedding frequency of the cylinder. There was an abrupt change in the phase angle between the lift force and the cylinder displacement near this shedding frequency.

Williamson and Roshko (1988) performed some pioneering forced-oscillation experiments to identify the wake patterns covering a range of amplitude-of-oscillation-to-diameter (A/d) ratios and a series of frequencies. The Reynolds number range was from about 300 to 1000. The wake patterns were identified as 2S, 2P, P + S, etc., for given values of oscillation frequencies and amplitude. The letter 'S' represents a 'single vortex' and the letter 'P' represents a 'vortex pair'. A 2S pattern, or mode, represents the shedding of a single vortex in each half-cycle of oscillation similar to the natural Karman vortex shedding. The 2P mode represents the shedding of two vortex pairs per shedding cycle. Fig. 1 shows the different types of modes observed for a given range of amplitude ratios and frequencies. (We will refer to the results in Fig. 1 as the W&R map.) In Fig. 1, λ represents the wavelength of oscillation, λ/d is equivalent to the reduced velocity U_R ($U_R = UT_e/d$), the period of excitation of the cylinder is T_e ($= 1/f_e$) and T_v ($= 1/f_v$) is the period of natural vortex shedding. In the preceding, d is the cylinder diameter, f_e is the excitation frequency, f_v is the vortex-shedding frequency, and U is the fluid approach velocity. The flow visualization studies of Williamson and Roshko (1988) agreed with the Bishop and Hassan (1964) results on the phase jump near resonance. Williamson and Roshko attributed the phase jump to the sudden transition from the 2S to 2P modes of vortex shedding. Blackburn and Henderson (1999) suggest that there remains some uncertainty in regard to the jump from the 2S to the 2P mode. Ongoren and Rockwell (1988) conducted experiments using the hydrogen bubble technique to study the timing of vortex shedding. They did not relate a change in phase of vortex shedding to a change in shedding mode. Nakano and Rockwell (1994) continued this research to study the flow structure in the frequency-modulated wake of a cylinder. They observed that, by modulating the frequency or by frequency deviation, it is possible to stabilize or destabilize the degree of organization of the vortices in the near wake.

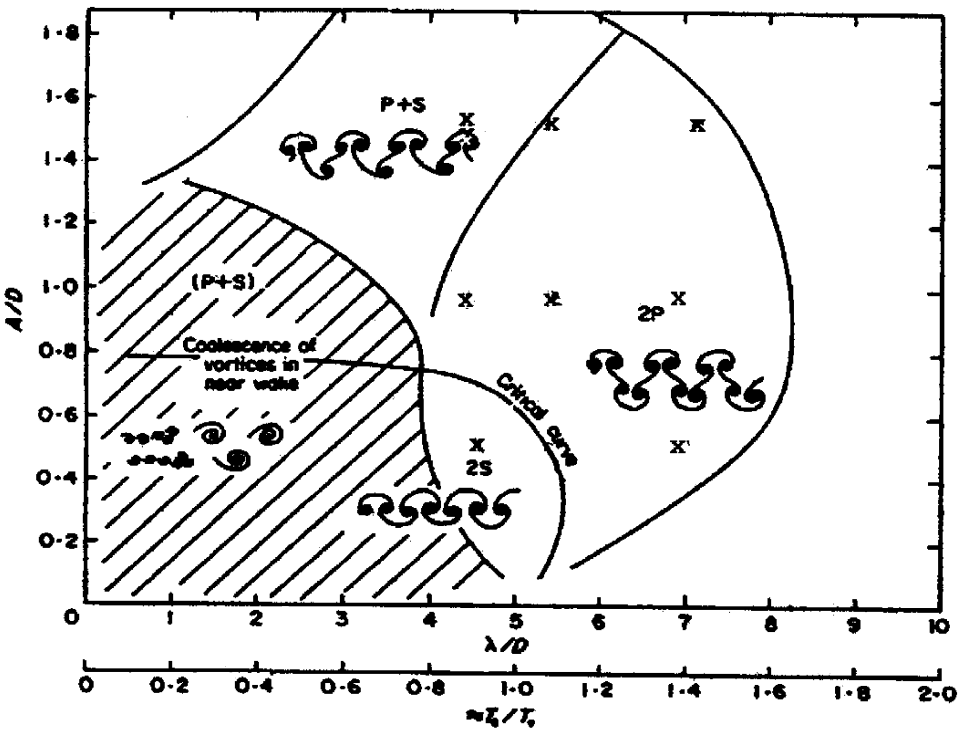

Fig. 1. Principal modes in the lock-in region of forced oscillation (from Williamson and Roshko, 1988). Cases examined herein are shown by X.

More recently, Gu et al. (1994) also undertook an experimental study of the timing problem. They noticed that, for a cylinder oscillating at a frequency lower than the natural shedding frequency, the vortices were shed when the cylinder had reached the maximum amplitude on the same side from which the maximum amplitude was reached. As the oscillation frequency was increased above the natural shedding frequency, the vortices were shed on the opposite side from which the maximum amplitude of the cylinder displacement was reached. Lu and Dalton (1996) confirmed these results numerically.

Feng (1968) studied VIV for air flow past an elastically mounted circular cylinder. The response behavior in his studies is fairly similar to the forced oscillation experiments. There were both high-amplitude and low-amplitude responses. Brika and Laneville (1993) and Govardhan and Williamson (2000) conducted similar experiments to those of Feng, but in water which produces a very different mass ratio effect. Both studies concluded that the lower amplitude response corresponds to 2S vortex shedding and the higher amplitude response corresponds to 2P vortex shedding.

Khalak and Williamson (1999) also repeated Feng's experiments in water at a different mass ratio. A larger synchronization range was observed compared to Feng's results. The initial branch of Khalak and Williamson represents a 2S mode and the lower branch represents a 2P mode. Blackburn et al. (2001) validated these results by using Direct Numerical Simulation (DNS) at $\mathrm{Re} = 500$.

Several recent CFD studies are relevant regarding the W&R map. A few studies at moderate Reynolds numbers will be discussed briefly. Lu and Turan (2000) examined the forced-oscillation problem for $\mathrm{Re} = 2000$. They observed that the wake had a 2P behavior at $f_v/f_e = 1.21$ for $A/d = 2$; this point on the W&R map is slightly above the 2P and P+S boundary in the region where no synchronized pattern exists. They also found, at $f_v/f_e = 2.0$, that there was no synchronized pattern which is consistent with the W&R map. At $f_v/f_e = 3.0$, they found a 3P pattern where the updated W&R map (Williamson and Govardhan, 2004) calls this structure the 2P+2S mode. These quite likely represent the same mode since each contains six vortices shed per cycle. Lu and Turan note their results at $\mathrm{Re} = 100$ agreed better with the experimental results of W&R. For $\mathrm{Re} > 1000$, they note that "quantitative differences occur although the qualitative flow field is still in close agreement with the experimental results". Lu and Turan attribute these differences to the fact that they did not use a turbulence model, even at $\mathrm{Re} = 2000$, and their calculations were 2-D which suggests that they could not capture the upper branch of the displacement versus reduced velocity plot. Regardless of these suggested shortcomings, there is quite likely a Reynolds number influence here also.

Guilmineau and Queutey (2004) considered an elastically mounted cylinder at low mass damping, oscillating transversely. They performed a 2-D numerical solution using primitive variables on a structured grid using $k-\omega$ Reynolds-averaged Navier–Stokes (RANS) modeling and a finite volume representation. The Reynolds number range was 900–15 000, the reduced velocity range was 1–17, the reduced mass was 2.4 and the mass-damping value was 0.013. A 2S mode was observed at $U_R = 3.63$ and $A/d = 0.34$ (initial branch), 2P (possibly) at $U_R = 4.51$ and 2S at $U_R = 11.0$ and $A/d = 0.95$ (upper branch), 2P at $U_R = 6.91$ and $A/d = 0.58$ (lower branch). The second and fourth of these results do not agree with the W&R map which again suggests a Reynolds number influence as Re increases.

Willden (2006) considered an undamped self-excited 2-D oscillation at $\mathrm{Re} = 10^4$ and $m^* = 2$, using large eddy simulation (LES) on an unstructured grid with a finite-element solution. He found the wake to be 2S (initial branch) at $U_R = 2.2$ and $A/d = 0.25$, 2P (lower branch) at $U_R = 5.9$ and $A/d = 0.55$, P+S at $U_R = 6.9$ and $A/d = 0.55$ and 0.4, and indeterminate (switching from P+S to 2P) on the upper branch. Again, these behaviors deviate somewhat from the W&R map, possibly because of the higher value of Re.

However, most of these results, both experimental and numerical, represent moderate Reynolds numbers. A typical practical scenario, like VIV of a riser on an offshore platform, would be at high Reynolds numbers and at a nonconstant frequency and amplitude, i.e., a self-excited oscillation.

1.2. Focus of this study

One objective of this study is to identify the differences in the wake structures of a periodic forced oscillation and a self-excited oscillation. A true VIV event does not have a controlled oscillation of the cylinder, and hence it is not meaningful to compare a periodic forced-oscillation case and a self-excited oscillation case. Our approach is to compare a periodic forced oscillation with a nonperiodic forced oscillation, both at constant amplitude. So, we seek further clarification to the differences between constant and variable frequency oscillations of a circular cylinder. Instead, while keeping the amplitude constant, the frequency of the periodic forced oscillation will be modulated to accommodate variable frequencies to achieve an effect a step closer to an actual VIV event. This kind of oscillation will have the dominant frequency and amplitude similar to that of a periodic oscillation but its instantaneous frequency differs from that of a pure sinusoidal oscillation. The vorticity contours for the various runs will be plotted and examined at different amplitudes, frequencies, and Reynolds numbers.

A second objective is to show that there is a Reynolds number influence on the vortex-shedding modes. We feel that we can demonstrate, using a 2-D calculation, that both effects influence the wake modes even though we are not capturing the complete details of the flow. Both of these considerations will provide an extended interpretation of the W&R map and complement other studies that have also provided further understanding of the W&R map.

In the present study, a 2-D uniform flow past a circular cylinder oscillating at a modulated frequency is numerically simulated. The Reynolds number range is 500–8000 and the wake turbulence is modeled by the Smagorinsky version of LES. The 2-D Navier–Stokes equations in a vorticity/stream-function form are solved using a finite-difference discretization. A second-order implicit Crank–Nicolson scheme for the diffusion terms and a third-order Adams–Bashforth scheme for time advancement are used in the solution.

We preface the discussion of our calculations with the reminder that our calculations are 2-D while the experiments represented in the W&R map are clearly 3-D. We obviously do not capture these 3-D effects with our 2-D simulations. Thus, we expect some influence on the results from this difference. However, the kinematics of a calculated 2-D flow field do not differ from the actual flow at a given axial position nearly as much as the calculated 2-D forces differ from the measured forces, especially at the relatively low Reynolds numbers representing the W&R map. So we expect that the calculated 2-D vortex patterns do have a reasonable measure of reality when compared to physical results at a given axial plane.

We do not always obtain the same mode behavior as shown on the W&R map for the same set of parameters in this set of comparisons. We attribute some of the differences to the fact that we are doing 2-D simulations; but some of the differences can also be attributed to the changes in Reynolds number. We note here that other investigators have also not found strict agreement with the W&R map.

2. Numerical studies of flow past a cylinder

In recent years, the forced-vibration problem and the VIV problem have been addressed using various computational procedures such as a discrete-vortex method, RANS equations, LES, DNS or a combination of different models.

LES involves a direct simulation of the dynamically important large-scale motions. The subgrid-scale turbulence model represents the effect of the unresolved small scales on the large scales. Many recent numerical studies, such as Beaudan and Moin (1994), Zhang (1995), Lu et al. (1997), Kravchenko et al. (1999) and Xu and Dalton (2001), conducted LES studies for 3-D flow past a fixed circular cylinder over a range of moderate values of Re and showed a similarity between the computed wake structures to those obtained from flow visualization studies. There have been more recent studies at higher Reynolds numbers, but these are not relevant to this effort.

Zhang and Dalton (1996) performed a 2-D LES numerical study at $\mathrm{Re} = 13\,000$ for transverse VIV. The results showed a reasonable agreement with the experimental measurements of the lock-in phenomenon. Dalheim (2000) conducted a 2-D numerical study to predict transverse VIV oscillation of a long riser using Strip Theory coupled with the technique of modal superposition. Saltara et al. (1998) performed a VIV study using a discrete-vortex/LES method at $\mathrm{Re} = 1000$ for a one degree-of-freedom (dof) problem. Tutar and Holdo (2000) found that a 3-D simulation is necessary for accurate results when the cylinder is vibrating. Al-Jamal and Dalton (2004) conducted a 2-D numerical simulation with LES modeling of a uniform approach-velocity flow past a circular cylinder undergoing VIV in the transverse direction. The calculated lock-in regime obtained by them found agreement with many experimental results for the case of moderate ratios of effective density of the cylinder to the fluid density. However, some disagreements were found for the cases of smaller ratios. These disagreements provided some of the impetus for the present study.

2.1. Governing equations

We will use the LES method with Smagorinsky subgrid scale modeling to represent the wake turbulence for the range of Reynolds numbers considered. The approach taken to calculate the flow field is similar to that of Zhang and Dalton (1996). A finite-difference scheme serves as a natural filtering operation with a filter width that is the width of the local grid size. The filtered 2-D governing equations are the Poisson equation for the stream function ψ,

$$\nabla^2\psi = -\omega, \tag{1}$$

and the vorticity transport equation

$$\frac{\partial\omega}{\partial t} + u\frac{\partial\omega}{\partial r} + \frac{v}{r}\frac{\partial\omega}{\partial\theta} = (\nu + \nu_t)\left(\frac{\partial^2}{\partial r^2} + \frac{1}{r}\frac{\partial}{\partial r} + \frac{\partial^2}{\partial\theta^2}\right)\omega, \tag{2}$$

where

$$u = \frac{1}{r}\frac{\partial \psi}{\partial \theta}, \quad v = -\frac{\partial \psi}{\partial r}, \quad \text{and} \quad \omega = \frac{1}{r}\frac{\partial (rv)}{\partial r} - \frac{1}{r}\frac{\partial u}{\partial \theta}. \tag{3}$$

In the equations above, r and θ are the dimensional coordinates in the physical plane, t is the dimensional time, v is the kinematic viscosity of the fluid, v_t is the turbulent eddy viscosity, u and v are the radial and circumferential velocity components, and ω is the vorticity. All of the flow variables are the filtered, or resolvable, quantities.

The effects of the turbulence are represented by an eddy viscosity v_t which is determined from a subgrid scale model. In the present study, we use the Smagorinsky model

$$v_t = (C_s \Delta)^2 \sqrt{2 S_{ij} S_{ij}} \tag{4}$$

where C_s is the Smagorinsky constant, Δ is the length scale (taken here to be the local mesh size), and S_{ij} is the strain rate tensor.

The fluid viscosity dominates over the turbulence as the wall is approached. A wall damping formulation, suggested by Van Driest (1956) is implemented such that the turbulence is damped exponentially. As a result, v_t will become

$$v_t = \left\{ C_s \Delta \left(1 - \exp\left[-\left(\frac{y^+}{26} \right)^2 \right] \right) \right\}^2 \sqrt{2 S_{ij} S_{ij}}, \tag{5}$$

where y^+ denotes the nondimensional normal distance from the cylinder surface in the inner region, $y^+ = y u_\tau / v$ with $u_\tau = (\tau_o/\rho)^{1/2}$, where τ_o is the wall shear stress.

The cylinder radius, R, and the steady approach velocity, U_∞, have been selected as the length and velocity scales, respectively, and the dimensionless time τ is tU_∞/R. The nondimensional governing equations are

$$\frac{\partial \omega}{\partial \tau} + u\frac{\partial \omega}{\partial r} + \frac{v}{r}\frac{\partial \omega}{\partial \theta} = \left(\frac{2}{\mathrm{Re}} + \frac{2}{\mathrm{Re}_t} \right) \nabla^2 \omega \tag{6}$$

and

$$\nabla^2 \psi = -\omega. \tag{7}$$

All of the terms in Eqs. (6) and (7) are now nondimensional. The Reynolds number and the turbulent (based on the turbulent eddy viscosity) Reynolds number are, respectively, $\mathrm{Re} = 2U_\infty R/v$ and $\mathrm{Re}_t = 2U_\infty R/v_t$ It is more convenient to solve this set of governing equations in a rectangular grid than a polar grid. Thus, the coordinate system is transformed to a rectangular system. The coordinate transformation, similar to the one used by Justesen (1991), is

$$r = 0.6e^{\xi} + 0.4 \ \text{ and } \ \theta = \pi\eta. \tag{8}$$

The physical and transformed planes are shown in Fig. 2.

We use the potential flow solution around a cylinder as the initial flow field. On the surface of the cylinder, the fluid velocity is equal to the velocity of the cylinder

$$v = \mathbf{v} \cdot \mathbf{t} \quad \text{and} \quad u = \mathbf{v} \cdot \boldsymbol{n}, \tag{9}$$

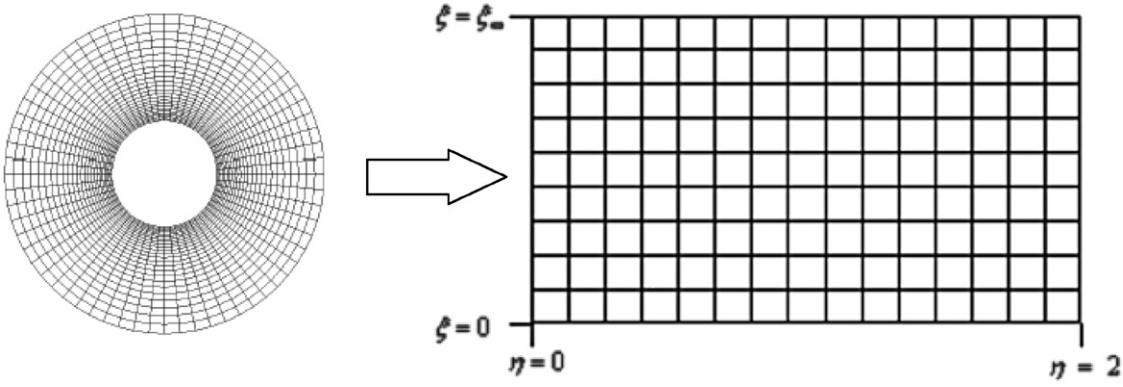

Fig. 2. Representation of the mesh in the physical domain and the computational domain.

where v and u are, respectively, the tangential and normal components of the velocity of the cylinder, $\mathbf{v}$ is the fluid velocity vector, and $\boldsymbol{t}$ and $\boldsymbol{n}$ are, respectively, the unit tangent and normal vectors of the moving cylinder surface. In the coordinate system that is attached to the cylinder, we have

$$v = u = 0. \tag{10}$$

2.2. Boundary conditions

On the surface of the fixed cylinder, $r = 1$, the boundary conditions are the no-slip and no-penetration conditions

$$\psi = -\frac{\partial \psi}{\partial r} = \frac{1}{r}\frac{\partial \psi}{\partial \theta} = 0. \tag{11}$$

The outer boundary conditions, as $r \to r_\infty$, are the combination of the Dirichlet boundary conditions, in the nonwake region

$$\left.\begin{aligned} &\psi = U_\infty\left(r - \tfrac{1}{r}\right)\sin\theta \\ &\omega = 0 \end{aligned}\right\} \tag{12}$$

and the vorticity extrapolation to the outer boundary by the vorticity projection method, the hybrid Neumann boundary conditions in the wake region (see Fig. 3)

$$\begin{aligned} &\frac{1}{r}\frac{\partial (ru)}{\partial r} + \frac{1}{r}\frac{\partial v}{\partial \theta} = 0, \quad \frac{\partial \omega}{\partial r} = \frac{\tan\theta}{r}\frac{\partial \omega}{\partial \theta}, \\ &\frac{1}{r}\frac{\partial^2 \psi}{\partial \theta^2} = \frac{\partial u}{\partial \theta}, \quad \text{and} \quad v = -\frac{\partial \psi}{\partial r}. \end{aligned} \tag{13}$$

The second of the conditions in Eq. (13) comes from $\partial\omega/\partial x = 0$ as $r \to r_\infty$, i.e., the streamwise gradient of vorticity is zero. The natural periodic boundary conditions are

$$\psi(r,\theta) = \psi(r,\theta + 2\pi) \quad \text{and} \quad \omega(r,\theta) = \omega(r,\theta + 2\pi). \tag{14}$$

The boundary condition for vorticity at the wall is obtained by extrapolating the calculated vorticity field adjacent to the surface, using a six-point extrapolation scheme.

The boundary conditions on the surface of the oscillating cylinder are changed due to the oscillatory motion of the cylinder and so are updated every time step in the calculation. These procedures are presented in greater detail in Al Jamal (2002) and Al Jamal and Dalton (2004). In brief, the governing equations are solved in a moving coordinate system attached to the oscillating cylinder. The inertia force that is present in such a system is subtracted from the calculated transverse force acting on the cylinder.

Since the cylinder is oscillating transversely, a modification must be made to the far-field boundary conditions. The entire coordinate system is allowed to move with the oscillatory velocity of the cylinder. This technique allows cylinder motion while keeping the mesh system unchanged. This technique was used by Lu and Dalton (1996), Zhang and Dalton (1996) and a similar technique was used by Blackburn and Henderson (1999) and others.

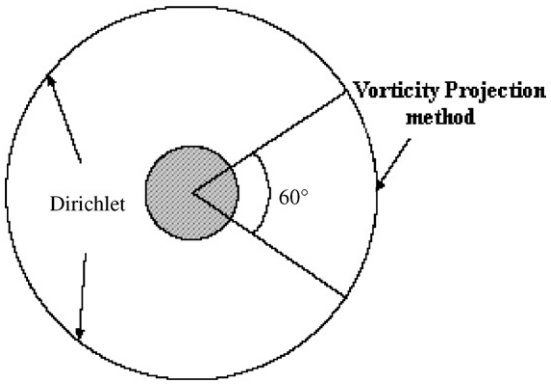

Fig. 3. The vorticity projection method.

The motion of the cylinder oscillating with constant frequency is given as

$$Y = A\ \sin(2\pi f_c \tau), \tag{15}$$

where A is the amplitude of oscillation and f_c is the base frequency (hereafter, carrier frequency) of oscillation. The description in Eq. (15) is referred to later as the *mod-zero* case. The motion of the cylinder oscillating with variable frequency is given as

$$Y = A\ \sin\left(2\pi f_c \tau + \frac{f_c - f_1}{f_1}\sin(2\pi f_1 \tau)\right), \tag{16}$$

where f_1 is a modulating frequency. This is referred to later as the *mod-one* oscillation. Multiple frequencies can be used to produce a more irregular frequency of oscillation as

$$Y = A\ \sin\left(2\pi f_c \tau + \sum_{i}^{I}\frac{f_c - f_i}{f_i}\sin(2\pi f_i \tau)\right), \tag{17}$$

where f_i represents the ith modulation frequency. This will be referred to later as a *mod-I* oscillation.

3. Results and discussion

Before proceeding to the results of the calculations of varying the Reynolds number with no modulation and modulating the frequency at different Reynolds numbers, it would be instructive to examine the results at a particular Reynolds number to see how the calculations compare with experimental results. Fig. 4 shows the drag and lift coefficients for a stationary cylinder at $\mathrm{Re} = 500$. The values of the coefficients are about 10% higher than the experimental values because of the 2-D representation of the flow in the calculations. The frequency of vortex shedding is captured quite well; the Strouhal frequency is 0.22 as compared to the experimental value of about 0.2 at $\mathrm{Re} = 500$.

Fig. 5 shows a comparison between the constant and variable frequency oscillations for $\mathrm{Re} = 500$ at $A/d = 0.5$ and 1.0. The influence is apparent. The modulation of the vibration frequency causes the time-response of the cylinder displacement to vary noticeably, especially at the larger times in both plots in Fig. 5.

Fig. 6 shows the drag and lift coefficients at both constant and variable frequency (modulated so that the deviations from the base frequency were small, regardless of the level of modulation).

3.1. Reynolds number dependence with no modulation

To illustrate the effect of Reynolds number, we have performed a series of calculations for Re values ranging from 500 to 8000 for $A/d = 0.5$, 1.0, 1.5, and 2.0 and $f_v/f_e = 0.88$, 1.1 and 1.36. Note that $f_v/f_e = T_e/T_v$ on the W&R map. All of these cases are shown in Table 1 and also indicated by X in Fig. 1 (the W&R map). Note that $A/d = 2.0$ slightly exceeds the maximum on the W&R map shown in Fig. 1, but the mode behavior at $A/d = 2.0$ can be determined. Each point (each set of A/d and T_e/T_v (or f_v/f_e) values) in Fig. 1 represents up to five Reynolds numbers as mentioned above. The W&R map does not represent the effects of Reynolds number greater than about 1000. It is the objective of this part of the study to consider higher values of Re. For purposes of comparison, we will consider three consecutive cycles of oscillation after the wake has been established and report the wake patterns for those cycles.

Fig. 7 shows the effect of changing the A/d value for $\mathrm{Re} = 500$ and $f_v/f_e = 1.1$. At $A/d = 0.5$, the mode pattern is 2S (Case 1 in Table 1); at $A/d = 1.0$, P + S (Case 3); at $A/d = 1.5$, P + S (Case 5); and at $A/d = 2.0$, P + S (Case 6). Modes of 2P are found on the W&R map for $A/d = 0.5$, 1.0, and 1.5, although the two extreme values are close to the 2S and P + S boundaries on the map, respectively. It is quite clear that increasing the A/d value changes the shedding modes, as is shown on the W&R map. However, the calculations yield a different set of shedding modes than shown on the map. Fig. 8 shows the effect of changing the frequency ratio for $\mathrm{Re} = 1000$ and $A/d = 1.0$ for a mod-two oscillation. Note that the change in mode behavior with increasing time in the respective cycles for each of the three cases. Each of these three cases on the W&R map falls in the 2P range. Only in the case of $f_v/f_e = 1.36$ did the results yield a 2P pattern. For $f_v/f_e = 1.1$, there was a consistent P + S pattern over three consecutive cycles. For $f_v/f_e = 0.88$, there was no consistent pattern over three cycles. About one cycle of oscillation is covered in the five frames shown in Figs. 7 and 8. Since the frequency is variable, it is difficult to compare these results in terms of cycles because each cycle is different.

Fig. 9 shows a comparison between the constant and variable frequency cases at four different Reynolds numbers for $f_v/f_e = 1.1$. At $\mathrm{Re} = 500$ and $A/d = 1.0$, the wake patterns are observed to be P + S, P + S, P + S (Case 3 in Table 1) for constant frequency and 2S, P + S, 2S (Case 4) for modulated frequency. At $\mathrm{Re} = 1000$ and $A/d = 1.0$, the wake patterns

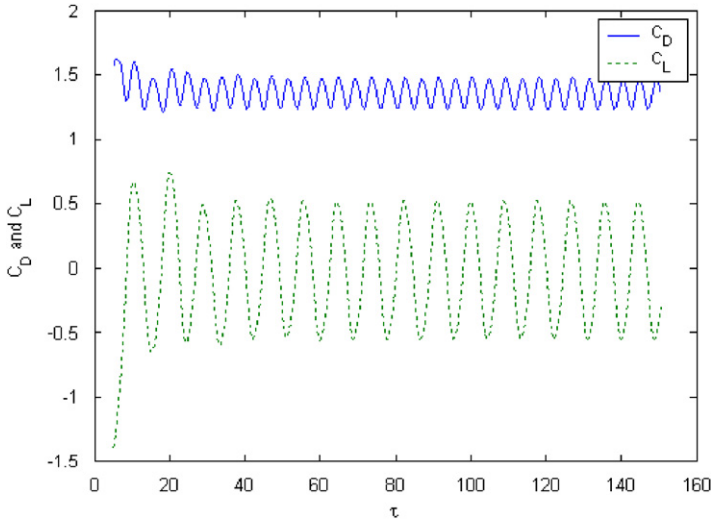

Fig. 4. C_D and C_L of the uniform flow past a stationary circular cylinder at Re = 500.

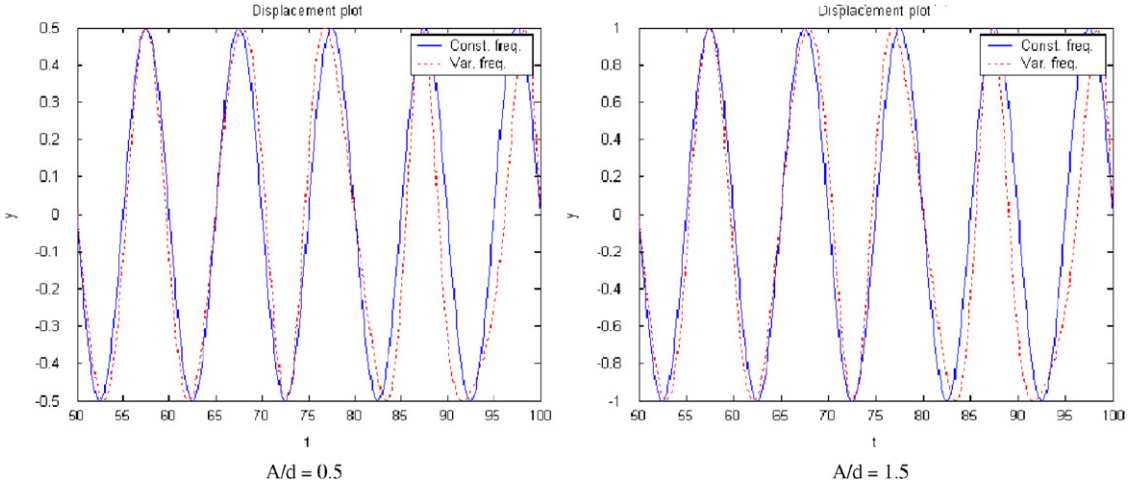

Fig. 5. Displacement plots for the forced oscillation of the cylinder at $A/d = 0.5$, 1.0, and $f_v/f_e = 1.1$ with $f_1 = 0.09$, $f_2 = 0.08$, and $f_3 = 0.07$.

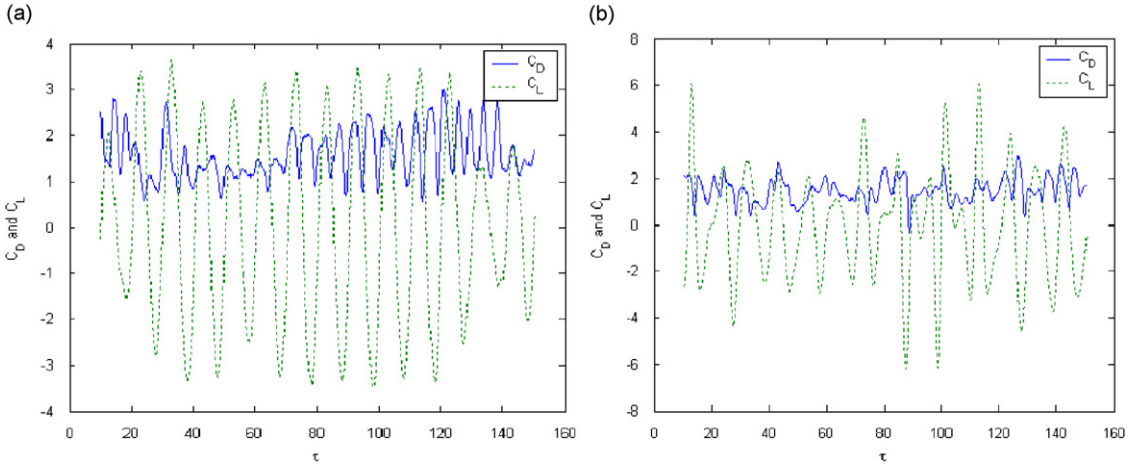

Fig. 6. C_D and C_L variation, Re = 3000, $f_v/f_e = 1.1$, $A/d = 1.0$: (a) constant-frequency case; (b) variable-frequency case. (Note the difference in ordinate scales.)

Table 1
The calculated results for all sets of parameters[a]

Case	Re	Amplitude ratio (A/d)	Base frequency, f_e (Hz)	Variable frequency, f_1 (Hz)	Variable frequency, f_2 (Hz)	Variable frequency, f_3 (Hz)	Modes of vortex shedding
1[b]	500	0.5	0.1	0	0	0	2S, 2S, 2S
2	500	0.5	0.1	0.09	0.08	0.07	2S, 2S, 2S
3[b]	500	1	0.1	0	0	0	P+S, P+S, P+S
4	500	1	0.1	0.09	0.08	0.07	2S, P+S, 2S
5[b]	500	1.5	0.1	0	0	0	P+S, P+S, P+S
6[b]	500	2	0.1	0	0	0	P+S, P+S, P+S
7	500	2	0.1	0.09	0.08	0.07	P+S, P+2S, P+S
8[b]	1000	0.5	0.1	0	0	0	2S, 2S, 2S
9	1000	0.5	0.1	0.09	0.08	0.07	2S, 2S, 2S
10[b]	1000	1	0.1	0	0	0	P+S, 2S, P+S
11	1000	1	0.1	0.09	0.08	0.07	2S, S, S
12	1000	1	0.1	0.06	0.04	0	S, 2P+2S, P+S
13[b]	1000	2	0.1	0	0	0	P+S, 2P, P+S
14	1000	2	0.1	0.09	0.08	0.07	2S, 2P, P+S
15[b]	3000	0.5	0.1	0	0	0	P+S, 2S, P+S
16	3000	0.5	0.1	0.09	0.08	0.07	2S, 2S, 2S
17[b]	3000	1.0	0.1	0	0	0	P+S, 2S, 2S
18	3000	1.0	0.1	0.09	0.08	0.07	2S, P+S, 2S
19[b]	6000	0.5	0.1	0	0	0	P+S, P+S, S
20	6000	0.5	0.1	0.09	0.08	0.07	P+S, 2S, 2S
21[b]	6000	1.0	0.1	0	0	0	P+S, 2S, 2S
22	6000	1.0	0.1	0.09	0.08	0.07	P+S, 2S, 2P
23[b]	8000	1.0	0.1	0	0	0	2S, P+S, 2S
24[b]	1000	1.0	0.081	0	0	0	2S, 2S, 2S
25	1000	1.0	0.081	0.01	0	0	2P+S, 2S, 2S
26	1000	1.0	0.081	0.02	0	0	2S, P+S, 2P+S
27	1000	1.0	0.081	0.03	0	0	P+S, 2S, 2P
28	1000	1.0	0.081	0.04	0	0	2S, P+S, 2S
29	1000	1.0	0.081	0.05	0	0	2S, 2S, P+S
30	1000	1.0	0.081	0.06	0	0	P+S, 2S, P+S
31	1000	10	0.081	0.06	0.04	0	P, P+S, P+S
32	1000	1.0	0.081	0.06	0.04	0.02	P+S, P+S, 2P
33[b]	500	1.0	0.125	0	0	0	2S, 2S, 2S
34	1000	1.0	0.125	0	0	0	2S, 2S, 2S
35	1000	1.0	0.125	0.06	0.04	0	P+2S, 2S, P+S
36[b]	500	1.5	0.125	0	0	0	2P, 2P, 2P
37[b]	1000	1.5	0.125	0	0	0	2P, 2P, 2P
38[b]	3000	1.5	0.125	0	0	0	P+S, P+S, P+S
39[b]	6000	1.5	0.125	0	0	0	P, 2P, 2P

[a] $f_v = 0.11$ for all cases: $f_e = 0.081$ yields $f_v/f_e = 1.36$; $f_e = 0.01$ yields $f_v/f_e = 1.1$; $f_e = 0.125$ yields $f_v/f_e = 0.88$.
[b] No Modulation.

differ more, showing P+S, 2S, P+S (Case 10) for constant frequency; and 2S, S, S (Case 11) and S, 2P+2S, P+S (Case 12) for two different modulated frequencies. For Re = 3000 and $A/d = 0.5$, the wake patterns continue to be affected with P+S, 2S, P+S (Case 15) for constant frequency and 2S, 2S, 2S (Case 16) for modulated frequency. At Re = 6000 and $A/d = 0.5$, the wake pattern differences continue with P+S, P+S, S (Case 19) for constant frequency and P+S, 2S, 2S (Case 20) for modulated frequency. The effect of the frequency modulation is quite clear. The wake patterns for a modulated frequency are noted to vary with time because the frequency is varying with time. We also note that the wake patterns in each case in Fig. 9 are distinct which shows a definite modulation effect on the wake modes.

For the no-modulation case, at $f_v/f_e = 1.1$ and $A/d = 1.0$, we obtained a 2S, 2S, 2S mode sequence at Re = 500 (Case 1) and 1000 (Case 2). The W&R map shows this point to be just inside the 2P pattern for $A/d = 0.5$ and well within the 2P region for $A/d = 1.0$. For $A/d = 1.0$, $f_v/f_e = 0.88$ and no modulation, the shedding patterns were 2S, 2S, 2S for both Re = 500 (Case 33) and 1000 (Case 34). Also at $f_v/f_e = 0.88$ and $A/d = 1.5$, we obtained 2P, 2P, 2P (Case 36)

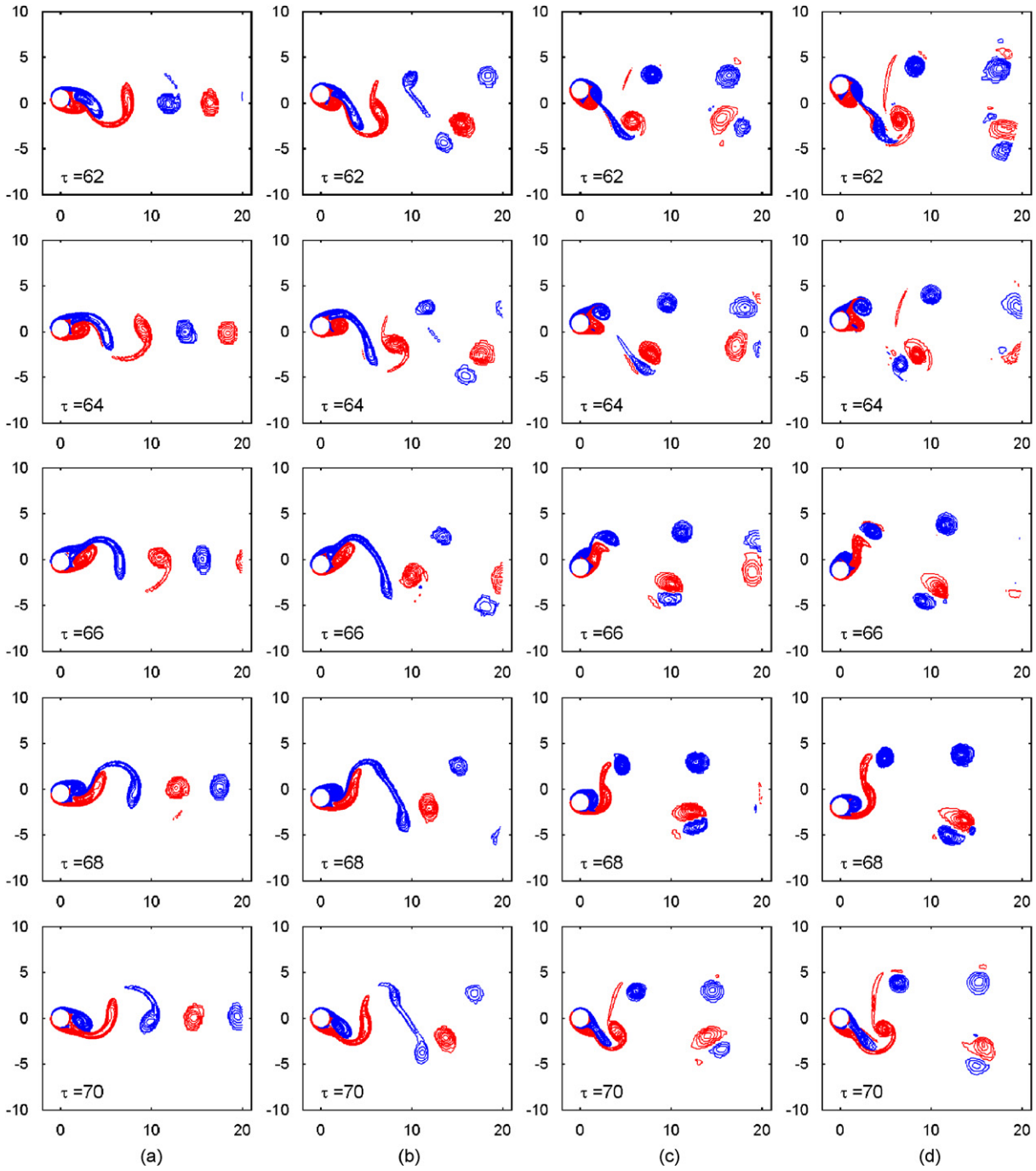

Fig. 7. Vorticity contours to study the effect of amplitude at Re = 500, $f_v/f_e = 1.1$: (a) $A/d = 0.5$, 2S (Case 1 in Table 1); (b) $A/d = 1.0$, P + S (Case 3); (c) $A/d = 1.5$, P + S (Case 5); (d) $A/d = 2.0$ P + S (Case 6).

at Re = 500; 2P, 2P, 2P (Case 37) at Re = 1000; P + S, P + S, P + S (Case 38) at Re = 3000; and P, 2P, 2P (Case 39) at Re = 6000. The W&R map shows a P + S pattern at this set of A/d and f_v/f_e values. Only at Re = 3000 and $A/d = 1.5$ did we get a match with the W&R map. This set of calculations show a clear Reynolds number dependence on the wake modes at this frequency range.

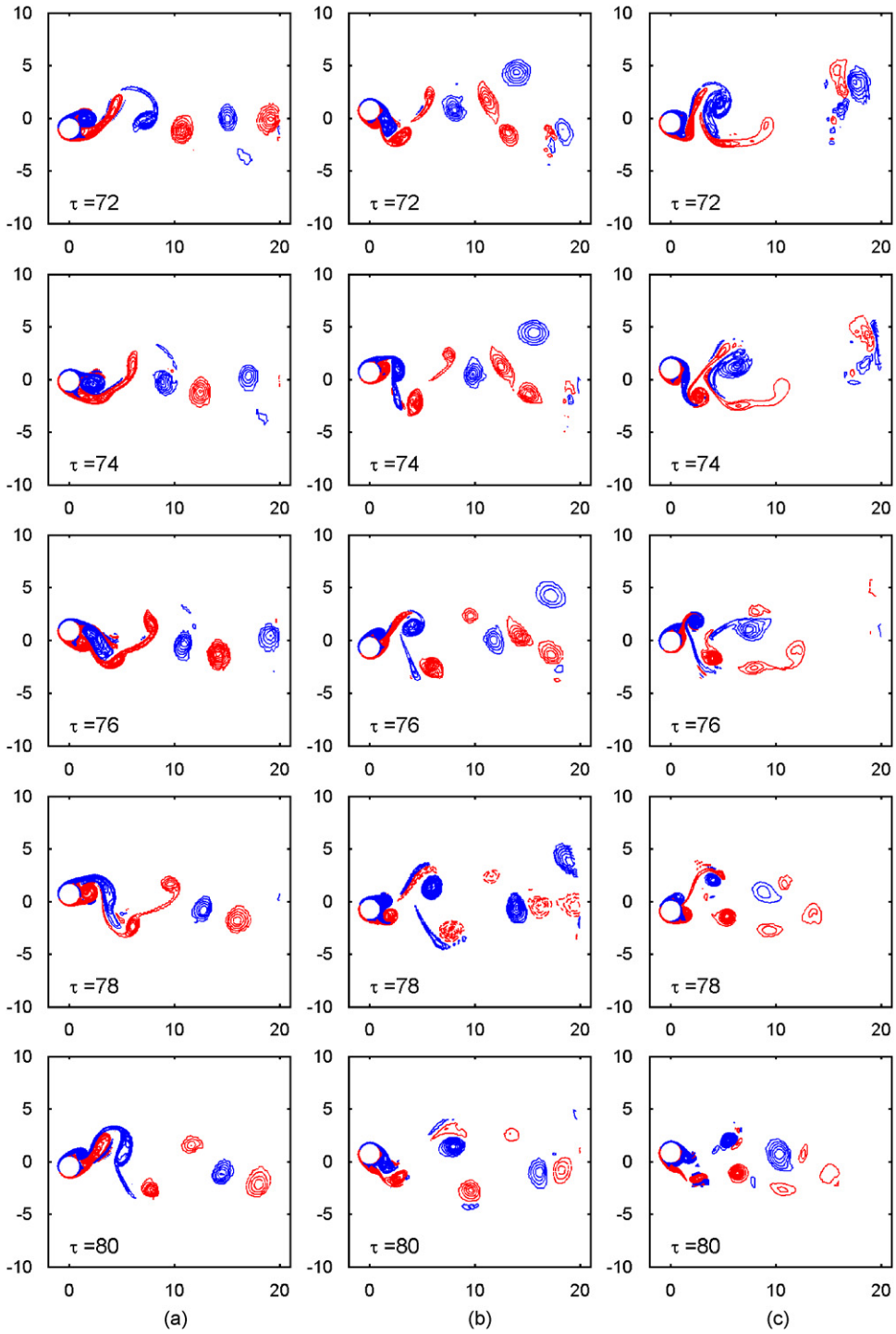

Fig. 8. Vorticity contours to study the effect of frequency variation at Re = 1000, $A/d = 1.0$: (a) $f_v/f_e = 1.36$, $f_1 = 0.06$, $f_2 = 0.04$ (Case 31 in Table 1); (b) $f_v/f_e = 1.1$, $f_1 = 0.06$, $f_2 = 0.04$ (Case 12); and (c) $f_v/f_e = 0.88$, $f_1 = 0.06$, $f_2 = 0.04$ (Case 35).

At $A/d = 0.5$ and $f_v/f_e = 1.1$, and no modulation, the vortex-shedding modes were consistently 2S at Re = 500 (Case 1) and 1000 (Case 8) for three consecutive cycles. At Re = 3000, the modes were P + S, 2S, P + S (Case 15) while at Re = 6000, the modes were P + S, P + S, S (Case 19). At the two higher values of Re, the mode patterns were

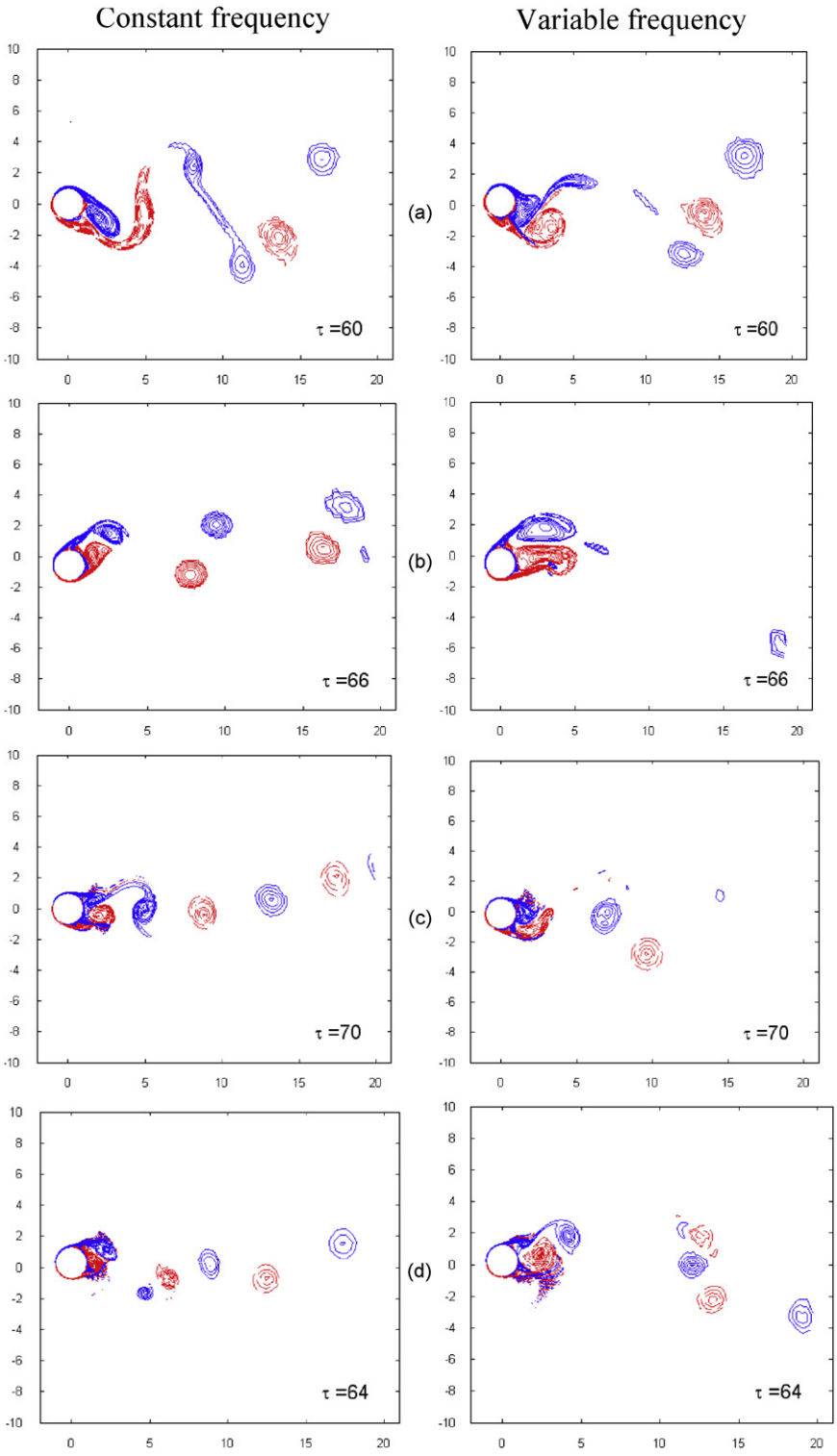

Fig. 9. Examples of the time differences in wake vorticity for several cases, each comparison is at the same time for $f_v/f_e = 1.1$: (a) Re = 500, $A/d = 1.0$ (Cases 3 and 4 in Table 1); (b) Re = 1000, $A/d = 1.0$ (Cases 10 and 11); (c) Re = 3000, $A/d = 0.05$ (Cases 15 and 16); (d) Re = 6000, $A/d = 0.5$ (Cases 19 and 20).

inconsistent, unlike those at the two lower values of Re. The W&R map shows a 2P pattern for this set of values of A/d and f_v/f_e, although this point on the map is very close to the line separating the 2S and 2P regimes. A Reynolds number effect seems to be responsible for these discrepancies with the W&R map.

At $A/d = 1.0$ and $f_v/f_e = 1.1$ again with no modulation, we obtained shedding modes of P + S, P + S, P + S at Re = 500 (Case 3); P + S, 2S, P + S at Re = 1000 (Case 10); P + S, 2S, 2S at Re = 3000 (Case 17); P + S, 2S, 2S at Re = 6000 (Case 21); and 2S, P + S, 2S at Re = 8000 (Case 23). The W&R map shows a 2P shedding pattern for this set of A/d and f_v/f_e values. Similar to the $A/d = 0.5$ results, this shows a definite Reynolds number influence as Re increases. The vortex modes do not have a consistent behavior at the two larger Re values.

For $A/d = 2.0$ and $f_v/f_e = 1.1$ and no modulation, we found that the shedding modes were P + S, P + S, P + S at Re = 500 (Case 6) and P + S, 2P, P + S at Re = 1000 (Case 13). From the W&R map, a P + S behavior might be expected for this condition, although this is somewhat speculative.

For $A/d = 1.0$ and $f_v/f_e = 1.36$ and no modulation (Case 24), the shedding patterns were P + S, P + S, and P + S for the three consecutive cycles of vortex shedding at Re = 1000. The W&R map shows a 2P pattern for this condition, although, as noted before, this point is somewhat close to the right extreme of the 2P regime.

Our observation for this set of calculations at these three different constant (unmodulated) frequencies is that there is a Reynolds number dependence on the vortex-shedding patterns for several cases. We also note that we did not reproduce the results in the W&R map except for the case of $A/d = 1.5$ and $f_v/f_e = 0.88$ at Re = 3000. In addition, the calculated results were somewhat close to those results shown in the W&R map at Re = 500.

3.2. Modulation dependence at different Reynolds numbers

We also allowed the frequency of oscillation to vary while keeping the oscillation amplitude constant for many of the cases considered in the variable Re study.

At $A/d = 0.5$, $f_v/f_e = 1.1$, and Re = 500, 1000, 3000, and 6000, we compared a constant frequency of oscillation (mod-zero) case with a modulated frequency with $f_1 = 0.09$, $f_2 = 0.08$, and $f_3 = 0.07$ (mod-three). At Re = 500 (Cases 1 and 2) and 1000 (Cases 8 and 9), we found a repeatable 2S pattern at both the mod-zero and mod-three cases. In other words, modulation had no effect at this low amplitude and low Re cases. The W&R map indicates a 2P mode is present for this case, although the point is very close to the line separating the 2S and 2P regimes. At Re = 3000, the mod-zero results shows P + S, 2S, P + S (Case 15) while the mod-three result shows 2S, 2S, 2S (Case 16) which clearly indicates an effect of frequency modulation. At Re = 6000, the mod-zero result shows 2S, P + S, 2S (Case 19) while the mod-three result shows P + S, 2S, 2S (Case 20). This latter case indicates essentially no effect of frequency modulation. The observation to be made here is that there is an effect on the vortex-shedding modes, but it seems to be a Reynolds number dependence rather than a dependence on the frequency at this low value of A/d.

Next, a comparison was made between the mod-zero and mod-three cases at $A/d = 1.0$, Re = 500, and $f_v/f_e = 1.1$. For mod-zero, we found P + S, P + S, P + S (Case 3) and, for mod-three, we found 2S, P + S, 2S (Case 4) in three consecutive cycles. This shows a dependence on the frequency change. When we increase A/d to a value of 2 at Re = 500 and $f_v/f_e = 1.1$, the mod-zero pattern is P + S, P + S, P + S (Case 6) and the mod-three pattern is P + S, P + 2S, P + S (Case 7). There is a very slight modification in the wake pattern for this frequency change.

We then compared the mod-zero, mod-two and mod-three cases at $A/d = 1.0$, Re = 1000, and $f_v/f_e = 1.1$. The mod-zero pattern is P + S, 2S, P + S (Case 10); the mod-two pattern is S, 2P + 2S, P + S (Case 12); and the mod-three pattern is 2S, S, S (Case 11). This comparison shows a clear dependence on modulation. We next increased the A/d value to 2.0 with Re = 1000 and $f_v/f_e = 1.1$. The mod-zero pattern is P + S, 2P, P + S (Case 13) while the mod-three pattern is 2S, 2P, P + S (Case 14). This comparison also shows a clear dependence on modulation.

We next increased Re to 3000 for $A/d = 1.0$ and $f_v/f_e = 1.1$. The mod-zero pattern is P + S, 2S, 2S (Case17) while the mod-three pattern is 2S, P + S, 2S (Case 18). Next, Re was increased to 6000, while keeping the same A/d and f_v/f_e values. The mod-zero result is P + S, 2S, 2S (Case 21) while the mod-three result is P + S, 2S, 2P (Case 22). This shows a slight Re dependence for like values of A/d and f_v/f_e.

The next frequency-modulated case is for $A/d = 1.0$ and Re = 1000 at $f_v/f_e = 1.36$ (mod-one). In the example, we let the value of f_1 increase from 0.0 to 0.06 in increments of 0.01 with $f_2 = f_3 = 0$. With $f_1 = 0.0$, the shedding mode is 2S, 2S, 2S (Case 24); at $f_1 = 0.01$, 2P + S, 2S, 2S (Case 25); at $f_1 = 0.02$, 2S, 2P + S, 2P + S (Case 26); $f_1 = 0.03$, P + S, 2S, 2P (Case 27); $f_1 = 0.04$, 2S, P + S, 2S (Case 28); $f_1 = 0.05$, 2S, 2S, P + S (Case 29); and $f_1 = 0.06$, P + S, 2S, P + S (Case 30). It is clear that there is a frequency dependence on the vortex-shedding modes. There is a continual change in the modes as the value of f_1 is increased. This sequence is shown in Fig. 10 in which there is a clear influence shown for the change in the modulation frequency.

The situation in the preceding paragraph is extended by further modulation of the frequency. First, we let $f_2 = 0.04$ (mod-two) with $f_1 = 0.06$ and $f_3 = 0.0$. This yields a vortex-shedding pattern of P, P + S, P + S (Case 31). Next, with f_2

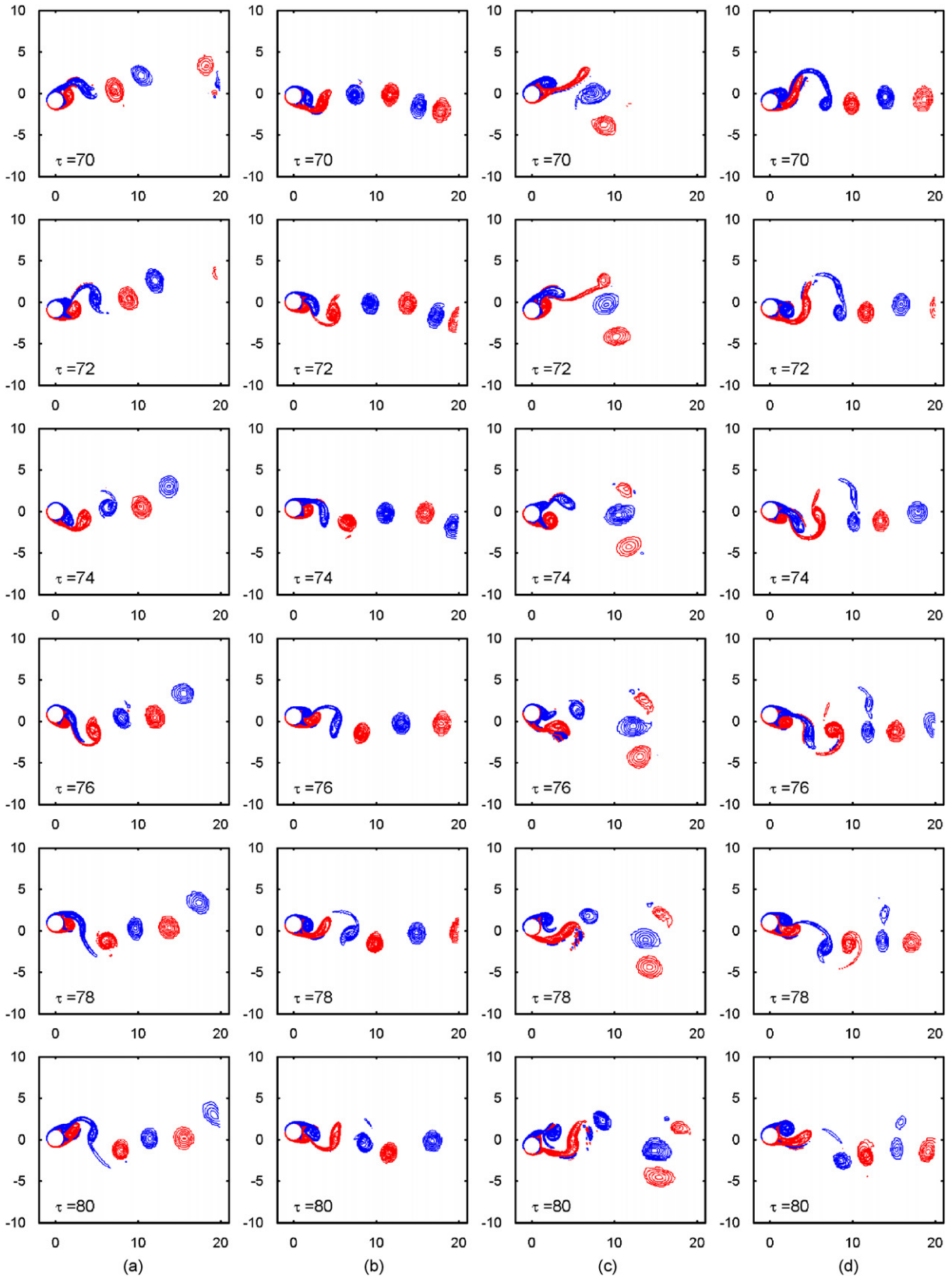

Fig. 10. Vorticity contours for the flow past an oscillatory cylinder at Re = 1000, $A/d = 1.0$ and $f_v/f_e = 1.36$: (a) constant frequency, 2S (Case 24); (b) $f_1 = 0.02$, 2S (Case 26); (c) $f_1 = 0.04$, P + S (Case 28); (d) $f_1 = 0.06$, 2S (Case 24).

still equal to 0.04, we let $f_3 = 0.02$ (mod-three); the vortex-shedding pattern becomes P + S, P + S, 2P (Case 32). Again, there is a clear frequency dependence on the shedding modes.

A summary of the modulated frequency comparisons indicates that there is a modulation influence in most cases and that there is no consistency in the wake patterns regarding frequency modulations. There appears to be no predictable trend to the results. It is not meaningful to relate these results to the W&R map since the frequency is a variable in the present study. Thus, we observe, in general, that the W&R mode patterns are not replicated when frequency variations are taken into account.

4. Conclusions

We have examined the influence of Reynolds number and frequency modulation on the constant-amplitude forced oscillation of a circular cylinder in a constant-velocity approach flow. Our calculations have been 2-D which do not provide for a precise comparison to experimental results. However, within the context of the 2-D calculations, the effect of the influence of oscillation frequency and Reynolds number on the wake mode behaviors can clearly be seen. We have found that there is an influence of Reynolds number when Re is increased to a value as high as 8000. The calculated wake modes do not agree with those in the W&R map except in some cases where Re and A/d are in the lowest ranges considered herein. We have also found that modulating the oscillation frequency at a constant-amplitude oscillation also has a distinct influence on the wake-mode behaviors. The base frequency was modulated by small increments with noticeable effects. Regardless of agreement with the W&R map, we found that modulating the oscillatory frequency clearly affects the vortex-shedding modes. However, we have not found a predictable trend regarding the effect of either Reynolds number or frequency modulation in the calculations we have performed. Thus, we suggest that there is a considerably more complicated nature of the wake patterns than is suggested by the Williamson and Roshko map for higher Reynolds numbers and for slightly variable frequency. There remains additional work to be done to clarify these issues.

Acknowledgements

The authors are grateful to RPSEA for providing financial support to the Center for Engineering Applications of Composites at UH for this project. TLC^2 at UH provided the computer support for this project for which we are grateful. The authors are grateful to the reviewers of the paper for their scrutiny because of which the paper has been improved.

References

Al Jamal, H., 2002. A 2-D numerical study with LES modeling of vortex-induced vibration of a circular cylinder in a uniform flow at moderate Reynolds number. Master's Thesis, Mechanical Engineering, University of Houston.

Al Jamal, H., Dalton, C., 2004. Vortex-induced vibrations using large eddy simulation at a moderate Reynolds number. Journal of Fluids and Structures 19, 73–92.

Beaudan, P., Moin, P., 1994. Numerical experiments on the flow past a circular cylinder at sub-critical Reynolds number. Report TF-62, Mechanical Engineering Department, Stanford University, USA.

Bishop, R.E.D., Hassan, A.Y., 1964. The lift and drag forces in a circular cylinder in a flowing fluid. Proceedings of the Royal Society of London A 277, 32–48.

Blackburn, H., Henderson, R., 1999. A study of 2-D flow past an oscillating cylinder. Journal of Fluid Mechanics 385, 255–286.

Blackburn, H., Govardhan, R.N., Williamson, C.H.K., 2001. A complementary numerical and physical investigation of vortex-induced vibration. Journal of Fluids and Structures 15, 481–488.

Brika, D., Laneville, A., 1993. Vortex-induced vibrations of a long flexible cylinder. Journal of Fluid Mechanics 250, 451–508.

Dalheim, J., 2000. A numerical procedure for prediction of interference and collision of multiple risers. In: Proceedings of the ETCE/OMAE/ASME Conference, February, New Orleans, LA, USA.

Feng, C.C., 1968. The measurement of vortex-induced effects in flow past stationary and oscillating circular and D-section cylinders. M.A.Sc. Thesis, The University of British Columbia, Vancouver, BC, Canada.

Govardhan, R., Williamson, C.H.K., 2000. Modes of vortex formation and frequency response for a freely-vibrating cylinder. Journal of Fluid Mechanics 420, 85–130.

Gu, W., Chyu, C., Rockwell, D., 1994. Timing of vortex shedding from an oscillating cylinder. Physics of Fluids 6, 3677–3682.

Guilmineau, E., Queutey, P., 2004. Numerical simulation of vortex-induced vibration of a circular cylinder with low mass-damping. Journal of Fluids and Structures 19, 449–466.

Justesen, P., 1991. A numerical study of oscillating flow past a circular cylinder. Journal of Fluid Mechanics 222, 157–196.

Khalak, A., Williamson, C.H.K., 1999. Motions, forces, and mode transitions in vortex-induced vibrations at low mass damping. Journal of Fluids and Structures 13, 813–851.

Kravchenko, A.G., Moin, P., Shariff, K., 1999. B-spline methods and zonal grids for simulations of complex turbulent flows. Journal of Computational Physics 151, 757–789.

Lu, X., Dalton, C., 1996. Calculation of the timing of vortex formation from an oscillating circular cylinder. Journal of Fluids and Structures 10, 527–541.

Lu, S., Turan, O.F., 2000. Numerical prediction of flow fields around circular cylinders: forced motion and dynamic response cases. ASME Journal of Fluids Engineering 122, 703–714.

Lu, X., Dalton, C., Zhang, J., 1997. Application of large eddy simulation flow past a circular cylinder. ASME Journal of Offshore Mechanics and Arctic Engineering 119, 219–225.

Nakano, M., Rockwell, D., 1994. Flow structure in the frequency-modulated wake of a cylinder. Journal of Fluid Mechanics 266, 93–119.

Ongoren, A., Rockwell, D., 1988. Flow structure from an oscillating cylinder. Part 1. Mechanisms of phase shift and recovery in the near wake. Journal of Fluid Mechanics 191, 197–223.

Saltara, F., Meneghini, J., Sigueria, C.R., Bearman, P., 1998. The simulation of vortex shedding from an oscillating circular cylinder with turbulence modeling. In: Proceedings of the ASME Conference on Bluff Bodies and Vortex-Induced Vibration, Washington, DC, USA.

Tutar, M., Holdo, A.E., 2000. Large eddy simulation of a smooth circular cylinder oscillating normal to a uniform flow. ASME Journal of Fluids Engineering 122, 694–702.

Van Driest, E.R., 1956. On turbulent flow near a wall. Journal of the Aeronautical Sciences 23, 1007–1011.

Willden, R., 2006. Numerical simulation of the multiple branch transverse response of a low mass ratio elastically supported circular cylinder. In: Proceedings, ASME PVP2006 Conference, Fluid-Structure Interaction Division, Vancouver, Canada.

Williamson, C.H.K., Govardhan, R., 2004. Vortex-induced vibrations. Annual Review of Fluid Mechanics 36, 413–455.

Williamson, C.H.K., Roshko, A., 1988. Vortex formation in the wake of an oscillating cylinder. Journal of Fluids and Structures 2, 355–381.

Xu, Y., Dalton, C., 2001. Computation of force on a cylinder in a shear flow. Journal of Fluids and Structures 15, 941–954.

Zhang, J., 1995. A numerical study of the three-dimensional unsteady flows past a circular cylinder. Ph.D. Dissertation, University of Houston.

Zhang, J., Dalton, C., 1996. Interaction of vortex-induced vibrations of a circular cylinder and a steady approach flow at $Re = 13{,}000$. Computers and Fluids 25, 283–294.